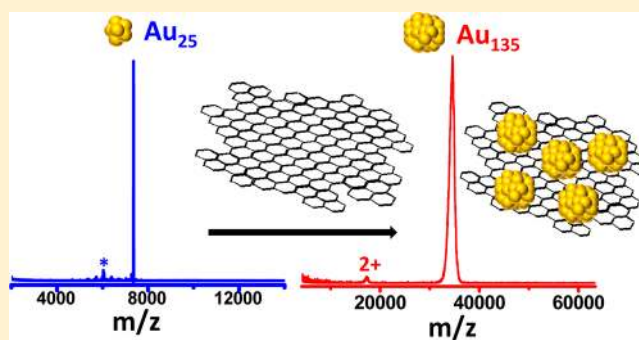# Coalescence of Atomically Precise Clusters on Graphenic Surfaces

Atanu Ghosh,[†] Thalappil Pradeep,[*,†] and Jaydeb Chakrabarti[‡]

[†]DST Unit of Nanoscience (DST UNS) and Thematic Unit of Excellence (TUE), Department of Chemistry, Indian Institute of Technology Madras, Chennai 600 036, India

[‡]S. N. Bose National Centre for Basic Sciences, Block-JD, Sector-III, Salt Lake, Kolkata 700091, India

Ⓢ *Supporting Information*

ABSTRACT: The interaction of ultrasmall metal clusters with surfaces of graphene is important for developing promising future applications of graphenic materials. In the experiment, chemically synthesized reduced graphene oxide (RGO) in water was mixed with $Au_{25}SR_{18}$ (where SR, SCH_2CH_2Ph, is a ligand protecting the cluster core) in tetrahydrofuran, and a completely new cluster, larger in mass, was formed at the liquid—liquid interface. Matrix assisted laser desorption ionization mass spectrometry of the product attached to RGO show that the peak due to $Au_{25}SR_{18}$ disappears gradually upon reaction and a single sharp peak referred to here as "135 ± 1 kDa cluster" appears. The composition of the new cluster

is very close to the well-known magic cluster, $Au_{144}SR_{60}$ while the peak maximum is at $Au_{135}SR_{57}$. The formation of 35 ± 1 kDa cluster from the parent Au_{25} is proposed to be governed by the trapping of smaller clusters in a deep potential well generated at the graphene surface. We theoretically model the active role of the surface in stabilizing the large clusters. Our studies indicate a general mechanism of stabilization of clusters of precise size via the competition between the interfacial fluctuations and the energy scales of interaction of the clusters with the surface. The chemical transformation occurs at deformable surfaces at reduced particle densities which is in good agreement with the theoretical model. Transformations of this kind are important in controlled tuning of particles at graphenic surfaces.

1. INTRODUCTION

Atomically precise ultrasmall clusters have different structural, electronic, magnetic, and catalytic properties compared to their bulk counterparts.[1−5] This makes studies of such clusters a growing area of nanoscience.[6−8] The interactions of ultrasmall metal clusters with graphenic surfaces are both pedagogically and technologically important for their ability to tailor the electronic and magnetic properties of graphene,[9,10] as required for many potential applications.[10−13] Very recently, graphene—metal and graphene—metal nanoparticle composites have become hot topics of research because of their biological, magnetic, electrochemical, optical, and environmental implications.[14−16]

Diffusion,[17,18] migration,[19] bonding,[20] and growth of transition metals on graphene[21] have been studied in detail. The mobility of naked clusters of palladium on graphene surfaces has also been studied.[22] The clusters of noble metals, protected with monolayers, referred to as quantum clusters (QCs), nanomolecules, or super atoms are stable materials with unusual optical, structural and catalytic properties[1,23−25] and such properties are modified by the monolayers.[26] Among the thoroughly studied noble metal clusters are $Au_{23}L_{16}$,[27] $Au_{25}L_{18}$,[28,29] $Au_{36}L_{24}$,[30] $Au_{38}L_{24}$,[31] $Au_{102}L_{44}$,[32] and $Ag_{44}L_{30}^{2}$ for which crystal structures are known (where L is the ligand protecting the cluster core). Interaction of naked noble metal clusters with supports, for example, magnesia has been well

studied and such supported clusters show unusual properties.[33−35] Molecular dynamics simulations predict that the cluster, Au_{140} undergoes Lévy-type power-law flight-length and sticking-time distributions on the basal plane of graphite.[18] However, the interaction of protected clusters or QCs with graphite as well as graphene is yet to be explored. The protecting monolayers are likely to affect the interaction between the graphite substrate and noble metal clusters. In particular, it is of immense interest how the stability and hence, the functionalities of these clusters be tuned over the graphite surface.

In the present work, we study the growth of noble metal clusters at graphenic interfaces. We use the large and atomically thin surface of graphene for the coalescence of $Au_{25}(SCH_2CH_2Ph)_{18}$ to 35 ± 1 kDa cluster (tentatively assigned as $Au_{135}(SCH_2CH_2Ph)_{57}$), where SCH_2CH_2Ph is a ligand protecting the cluster core of finite number of gold atoms. We will refer to these molecules as Au_{25} and Au_{135} in the subsequent discussion. We observe that the conversion takes place on the graphene surface via a sluggish dynamics, and it depends on both graphene and Au_{25} concentrations.
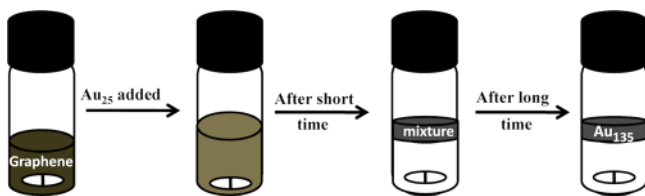
2. EXPERIMENTAL METHODS

Synthesis of Graphene. Details about the synthesis of graphene have been presented in the experimental section (Supporting Information S1). Brifely, graphene oxide (GO) was prepared by the modified Hummer's process.[36] Then GO was reduced to reduced graphene oxide (RGO) by hydrazine.

Synthesis of Au$_{25}$. We have prepared the parent material Au$_{25}$, by our in-house-developed method. The concept of slow reduction was used to prepare this material. To HAuCl$_4$ in a methanol−tetrahydrofuran (THF) mixture (100 mg, 25 mM), 3 equiv of phenylethanethiol (SCH$_2$CH$_2$Ph) was added under stirring at room temperature. After 30 min, 10 equiv of ice cold solution of NaBH$_3$CN in 2 mL of cold water was added and the solution was kept stirring at room temperature. Evolution of Au$_{25}$ was investigated by time dependent MALDI MS study using DCTB (*trans*-2-[3-(4-*tert*-butylphenyl)-2-methyl-2-propenylidene]malononitrile) as the matrix. This matrix is important to get clusters without fragmentation as reported previously.[37]

Reaction of Graphene with the Au$_{25}$ Cluster. About 100 μL of as-synthesized Au$_{25}$ in tetrahydrofuran (THF) was added to a 3 mL suspension of chemically synthesized graphene[36] (0.01 wt %) in water, which was thoroughly cleaned and contained no impurities. Rapid disappearance of the color of the mixture was noticed and almost simultaneously a black matter suspended at the top. The aqueous phase became colorless. Time dependent MALDI MS study of this black suspended matter was performed. Initial MALDI MS measurement of this matter shows the presence of different cluster masses. After a long time (120 min), for a required amount of cluster and graphene (0.01 wt %), we got a single peak in MALDI MS. In Scheme 1, we show a cartoon representation of this reaction.

Scheme 1. Schematic Representation of the Reaction of Au$_{25}$(SCH$_2$CH$_2$Ph)$_{18}$ with Aqueous Suspension of Graphene[a]

[a]A magnetic pellet used for stirring is shown at the bottom of the glass bottle, used for synthesis.

UV−vis Measurement. PerkinElmer Lambda 25 UV−vis spectrometer was used for the measurements. Spectra were typically measured in the range of 190−1100 nm.

MALDI MS Measurement. The mass spectrometric studies were conducted using a Voyager DE PRO Bio spectrometry Workstation (Applied Biosystems) MALDI TOF MS instrument. A pulsed nitrogen laser of 337 nm was used for desorption ionization and TOF was operated in the delayed extraction mode. Typical delay times employed were of the order of 75−150 ns. The mass spectra were collected in the positive ion mode and were averaged for 200 shots. Most of the measurements were done in the linear mode. To study the evolution of Au$_{25}$ by MALDI MS, 1.5 μL of the reaction mixture was taken out during its synthesis and mixed with 2.5 μL of DCTB matrix, prepared in toluene. The mixture was

spotted on the target plate. The plate was left to dry in air and inserted into the spectrometer. It was assumed that after spotting that there was no progress in the reaction.

In the case of the black suspended matter (during Au$_{25}$−graphene reaction), each time, a small amount of the product (graphene and the cluster) was taken out using a 10 μL pipet tip. Then the material was mixed with freshly prepared 2.5 μL of toluene solution of DCTB. The sample was dried in air and inserted into the spectrometer.

TEM Measurement. TEM images were collected using a JEOL 3010 microscope. A diluted solution of Au$_{25}$ was spotted on carbon coated copper grid and was dried in laboratory ambience. Images were collected at 200 keV. In the case of the black suspended matter, a small amount of it was taken out from the bottle and spotted on the grid. It was dried in laboratory ambience.

3. RESULTS AND DISCUSSION

As Au$_{25}$ has been characterized in great detail previously[38] by various studies, we present only essential details here. Typically, the samples are characterized by their well-defined optical absorption features.[1] The positions of peak maxima, peak shape, and intensities are specific to Au$_{25}$(SCH$_2$CH$_2$Ph)$_{18}$ in THF (Figure 1). As the spectrum of Au$_{25}$(SCH$_2$CH$_2$Ph)$_{18}$ has

Figure 1. UV−vis spectrum of the as-synthesized sample. The spectrum matches with the reported spectrum of Au$_{25}$(SCH$_2$CH$_2$Ph)$_{18}$.[1] Inset: MALDI MS spcetrum of the sample in the positive ion mode. The peak at *m/z* 7391 confims the formation of Au$_{25}$(SCH$_2$CH$_2$Ph)$_{18}$. The fragmented product, Au$_{21}$(SCH$_2$CH$_2$Ph)$_{14}^+$ is shown with an asterisk (*).

been discussed thoroughly, we merely note that the spectrum is comparable to the published data.[1,37,38] The purity of the sample is proven by its unique MALDI MS spectrum (inset of Figure 1), showing a narrow ($\Delta m = 15$) peak at 7391 due to Au$_{25}$(SCH$_2$CH$_2$Ph)$_{18}^+$ along with its characteristic fragmentation product at *m/z* 6055 due to Au$_{21}$(SCH$_2$CH$_2$Ph)$_{14}^+$, as mentioned previously.[37] The data were collected at threshold laser intensity to reduce fragmentation. Formation of Au$_{25}$ was completed after 36 h of stirring (Figure S2). Chemically synthesized graphene samples were characterized in the solution phase by optical absorption spectroscopy and in the drop-cast form by transmission electron microscopy (data to be presented later).

MALDI MS of the black suspended material formed by the reaction between Au_{25} and graphene is shown in Figure 2. This
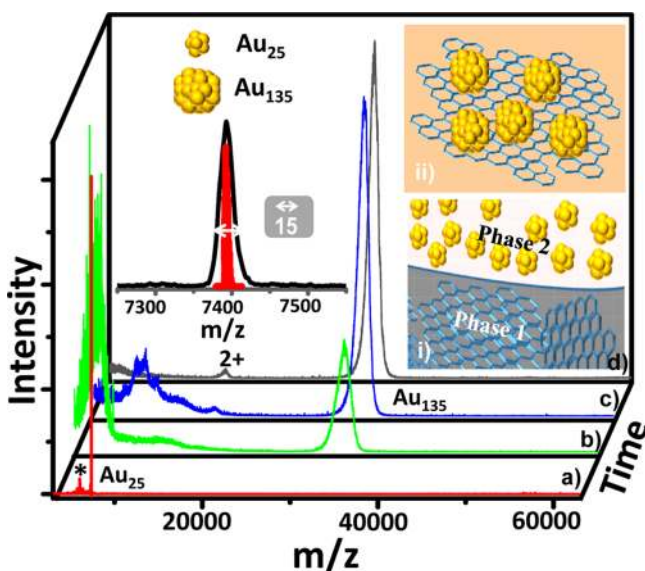

Figure 2. (a−d) Time dependent positive ion MALDI MS study of the conversion of Au_{25}. At zero time (a) a peak corresponding to pure Au_{25} (main peak at m/z 7391 and a fragment at m/z 6055) is seen. The fragment is shown with an asterisk (*). The main peak is expanded on the top. After 15 min, mixtures of clusters, including Au_{135} were formed (b). With increasing time, the peak of Au_{135} increases and peaks corresponding to lower m/z decrease in intensity (c). (d) Spectrum shows that Au_{135} has been formed after 120 min for a mixture of 0.01 wt % graphene (3 mL) and 27 μM Au_{25} (100 μL). Dication (2+) of Au_{135} is seen in MALDI MS, marked on trace (d). Insets: (i) The presence of two phases of the reaction mixture, cluster (Au_{25}) and graphene; and (ii) the final product of Au_{135} on the graphene surface.

transformation shows a gradual evolution of a peak at m/z 34.4 kDa assigned to $Au_{135}(SCH_2CH_2Ph)_{57}^+$ along with the simultaneous disappearance of the peak due to $Au_{25}(SCH_2CH_2Ph)_{18}^+$. The assignment of

$Au_{135}(SCH_2CH_2Ph)_{57}^+$ may have a slight uncertainty as other Au/SCH_2CH_2Ph combinations are possible (see below). We have seen a dication, assigned to $[Au_{135}(SCH_2CH_2Ph)_{57}]^{2+}$ at m/z 17.2 kDa, which further supports the assignment. Occurrence of dication is a standard feature seen in MALDI MS of such large clusters.[39] However, as mass measurements at this mass range have some inaccuracy, it is safe to describe these clusters as "35 ± 1 kDa clusters".

One may wonder whether the new mass peak at 34.4 kDa is an adduct of $Au_{25}(SCH_2CH_2Ph)_{18}$ with graphene as such ultrathin sheets are expected to wrap around a cluster. This possibility was investigated. Graphene sheets prepared are of different sizes (to be seen below from the TEM data) and obviously the adduct peaks derived from them should be composed of multiple maxima, reflecting the polydispersity of graphene in a given preparation. Also at higher laser powers, such peaks are expected to fragment, giving carbon or carbon cluster losses which were not observed. Multiple preparations of graphenes produced the same peak. These made us conclude that graphene is not part of the mass peak. Larger width of the peak in comparison to the narrow peak of Au_{25} was a concern. To find out whether this is due to the inherent reduction in resolution at higher masses in a liner time-of-flight measurement, the spectra of similar samples at higher masses were compared. MALDI MS spectra of gold clusters of lysozyme $(Lyz)^{40}$ and parent Lyz are shown in Figure S3. These comparisons suggest that the observed peak is due to single cluster. The broadness of the feature is due to reduced instrumental resolution at high masses as revealed from the protein mass spectrum (Figure S3).

It is important to point out that MALDI MS was measured at threshold laser powers which result in spectra at no or reduced fragmentation.[37] This complete conversion occurs at a finite time interval (more details are below) after which no Au_{25} was detected in the solution, at the interface. In between these two times, several features were observed in the lower mass region (m/z 8000−18000) which are attributed to intermediate products. From our time dependent study, we have shown that Au_{33}, Au_{38}, Au_{55}, and some other clusters (the ligand shell is neglected in this description) were formed at the lower mass
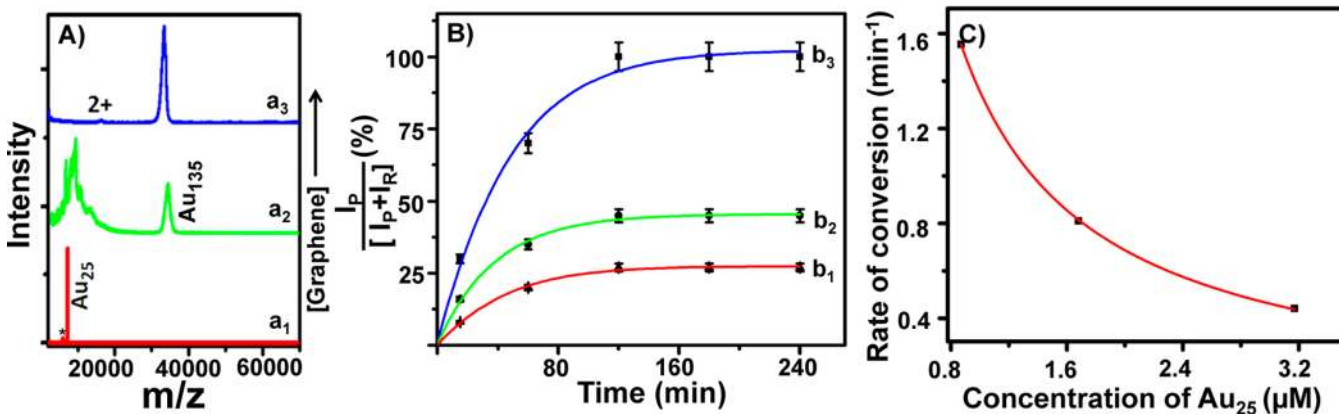

Figure 3. (A) MALDI MS spectra with increasing graphene concentration for a constant Au_{25} concentration. (a_1) Data corresponding to Au_{25} alone. The peak marked * is due to the fragment, $Au_{21}L_{14}^+$. (a_2) Data at lower concentration (0.005 wt %) of graphene where complete conversion of Au_{25} to Au_{135} has not taken place. It shows some peaks at lower mass. (a_3) At higher concentration (0.01 wt %) of graphene, complete conversion to Au_{135} has happened. Both the spectra were collected after 180 min of mixing the reactants. Dication of Au_{135} is marked on the above figure. (B) Time dependent conversion of Au_{25} for a fixed graphene concentration at different Au_{25} concentrations. I_P and I_R represent the intensity of Au_{135} and Au_{25} in the MALDI MS spectra. Traces b_1, b_2, and b_3 represent final concentrations of Au_{25} in solutions (3.17, 1.68, and 0.87 μM, respectively). Statistics refer to data from multiple measurements. (C) A plot of slope vs surface concentration derived from panel B.

C

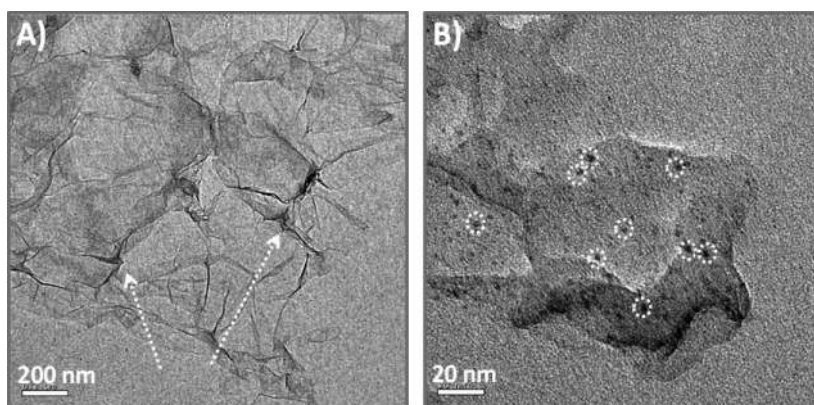dx.doi.org/10.1021/jp503001s | J. Phys. Chem. C XXXX, XXX, XXX−XXX

Figure 4. (A) TEM image of chemically synthesized graphene alone. The nanometer thin folding (marked) indicates that the sheets imaged contain two-three layers of chemically synthesized graphene. (B) Image of graphene surface containing clusters (Au_{135}). Some clusters are marked with circles. Outside the graphene surface, there was no cluster. It proves that the conversion happened only on graphene surfaces. Number of folding has decreased significantly in panel B.

region during the conversion process (Figure S4). This confirms that the transformation is nonstoichiometric. The product ion, $Au_{135}(SCH_2CH_2Ph)_{57}^+$ has much larger width than $Au_{25}(SCH_2CH_2Ph)_{18}^+$ due to distribution in ligand composition as well as reduced resolution at the higher mass range. Due to this reason, the exact composition of the product may have some variation. A stable cluster known in this mass range is $Au_{144}(SCH_2CH_2Ph)_{60}$. Actual mass of $Au_{144}(SCH_2CH_2Ph)_{60}$ is 36.5 kDa as measured by electrospray ionization mass spectrometry (ESI MS). But MALDI MS for the product shows a peak around ~34 kDa.[41] It is likely that $Au_{144}(SCH_2CH_2Ph)_{60}$ with some fragmentation is observed here. Although the exact composition of the product is uncertain, we note that only one product was seen.

The transformation is sensitive to both concentration of the cluster and graphene. For a given cluster concentration, increasing graphene content converts all the clusters to Au_{135}. As shown in Figure 3A, at a lower graphene concentration (0.005 wt %, trace a_2), Au_{25} is observed even after 48 h of reaction. At higher concentration (0.01 wt %, trace a_3) of graphene, conversion to Au_{135} takes place where the Au_{25} peak is not any more visible. Further, upon increasing cluster concentration, for a fixed graphene concentration (0.01 wt %), we see reduced conversion (Figure 3B). While at lower cluster concentration all the clusters convert to Au_{135}, at increasing cluster concentration, more clusters remain without conversion. This reduced efficiency of conversion continued even upon a longer reaction time.

While the transformed clusters are less susceptible for electron beam-induced aggregation, the parent Au_{25} is extremely sensitive to electron beam-induced aggregation and undergoes rapid coalescence (Figure S5). Smaller clusters such as Au_{25} grow in size with exposure to electron beam.[42] The molecular nature of Au_{135} is evident in the mass spectrum which exhibits a well-defined peak assigned to a specific composition. From the MALDI MS study, we have seen that Au_{135} is resistant toward fragmentation upon increasing laser intensity used to perform desorption-ionization (Figure S6). Generally, clusters show severe laser intensity-dependent fragmentation in which more of lower mass ions are observed at increasing laser fluence. The increased stability observed is due to the fact that the clusters are attached to the graphene surface which efficiently removes the excitation energy.

The slope of the curves in Figure 3B gives the rate of conversion to Au_{135} at different times. The rate is rapid at initial times, slows down gradually, and finally becomes zero at very large times. The low time values of the rate of conversion, k, have been plotted as a function of the Au_{25} surface concentration, c, on the graphene surface (Figure 3C). The best fitted line shows that $k = \lambda/c$, the dynamical information being incorporated in λ which has the dimension $[L^2T]^{-1}$. Such dynamical quantity is dimensionally consistent with mean squared displacement (MSD) $\langle r^2 \rangle \propto t^{-1}$ over the surface as a function of time, t. Such MSD can be found if the particle motion is in a trapping potential of strength V_0 in the presence of strong damping Γ. The mean squared fluctuations from the trapping center would decay as $[1 + (V_0/\Gamma) t]^{-1}$. Clearly the formation of Au_{135} clusters from the parent Au_{25} clusters is governed by the trapping of the smaller clusters in a deep potential well generated by the graphene surface.

Figure 4 compares the TEM images of chemically stable graphene and gold cluster-nucleated graphene. The size of Au_{135} is in the 2 nm range which agrees with the observed particle sizes, which are the expected sizes of clusters of this range.[39] Number of folds of the sheets has reduced after the reaction (Figure 4B). As the clusters are strongly adherent to the graphene surface, our efforts to separate Au_{135} in solution for additional examination was unsuccessful.

The energy gain due to reduction of the surface curvature may be the main drive to trap the smaller clusters, leading to their coalescence, as suggested by the concentration dependence of the conversion rate. In the following we present a general mechanism of stabilization of clusters of precise size via the competition between the interfacial fluctuations and the energy scales of their interaction with the surface. Let us assume that the small clusters are driven by the curvature. The smaller clusters thus experience a chemical potential proportional to the local curvature on the surface. Let $h(\vec{r})$ be the height of the surface and $\rho(\vec{r})$ be the density of the smaller clusters on the surface at a point $\vec{r}$. The chemical potential experienced by the smaller clusters is then $\mu(\vec{r}) = \lambda \vec{\nabla}^2 h(\vec{r})$, λ being the coupling parameter. We use the density functional free energy for a strongly interacting classical system,[43] consisting of the smaller clusters and the surface. The Gibbs free energy of the system consists of several components: The entropy of the smaller clusters given by $\int d\vec{r}\rho(\vec{r}) \ln(\vec{r})$; the entropy of height fluctuations of the surface $\int d\vec{r}h(\vec{r}) \ln h(\vec{r})$;

the contributions due to correlated changes in density of the smaller clusters and in the surface height, given by $-(1/2) \int d\vec{q}\, c(\vec{q})|\delta\rho(\vec{q})|^2$ and $-(1/2) \int d\vec{q}\, \alpha(\vec{q})|\delta h(\vec{q})|^2$, respectively. The wave vector modes $\delta\rho(\vec{q})$ and $\delta h(\vec{q})$ indicate heterogeneity with respect to the mean density and average surface height, while $c(\vec{q})$ and $\alpha(\vec{q})$ denote their correlations, respectively. Finally we add the contributions due to the chemical potential coupling between the smaller clusters and the surface, resulting in $\int \mu(\vec{r})\delta\rho(\vec{r})\, d\vec{r}$. The net free energy F of the system is given by the sum of these contributions. The equilibrium heterogeneity of the structure spontaneously supported by the system is given by the simultaneous conditions $\partial F/\partial\rho(\vec{q}) = \partial F/\partial h(\vec{q}) = 0$. We consider the standard Ornstein–Zernike form for the correlation functions:[43] $c(q) = c_0/(q^2 + \xi_0^2)$, ξ_0 being the particle correlation length and c_0 related to the inverse of the bulk compressibility; and similarly $\alpha(\vec{q}) = \alpha_0/q^2 + \xi_s^2$; ξ_s being the correlation length of the surface height fluctuations and α_0 given by the inverse of surface compressibility. For large λ, $L \approx q^{-1} \propto \lambda\xi_0/c_0^{1/2}$, for a given concentration of graphene. At very low particle densities, $c \approx 1$, the correlation length typically extends to a few particle diameters so that L is about a few nanometers so far as λ is a finite number. L compares well to the size of Au_{135} clusters. The theory of interacting fluids shows[43] that $c_0 \approx -\infty$ for a high density incompressible fluid and c_0 decreases with decreasing particle density. Thus, lower density of the particles facilitates the formation of bigger clusters which is qualitatively supported by the experimental observations. On the other hand, λ can be taken to increase with increasing graphene concentration so that the stabilization of large clusters would be favored, as found in the experiments.

Our phenomenological model hints at the most dominant factors underlying the experimental observations. This also indicates what aspects should be looked into in ab initio calculations. We must add here that the dynamics of the system can be captured only within Carr–Parinello type ab initio calculations which are too expensive to carry out, unless the specific aspects of the phenomenon are known from simplistic calculations. We know that the system under discussion is not a metal particle alone; it has a molecular shell. Nevertheless, it is a particle on a deformable surface. The dynamics of such a complex system in its simplest form is considered here.

4. CONCLUSION

In summary, we established the coalescence of clusters of finite size to form a larger cluster at graphenic interfaces. In particular, the role of the interface has been ascertained by both experiments and model theoretical calculations in stabilizing the large clusters. Our methodology with diverse clusters and high surface area substrates will allow the creation of atomically precise clusters directly on such supports. Extension of this study to fullerene and carbon nanotubes may be useful to produce new clusters. Such materials are expected to have novel applications via controlled tuning of the structural and electronic properties of both the deposited clusters and the support surfaces.

■ ASSOCIATED CONTENT

ⓈSupporting Information

Figure S1–S6 are included. This material is available free of charge via the Internet at http://pubs.acs.org.

■ AUTHOR INFORMATION

Corresponding Author
*E-mail: pradeep@iitm.ac.in.

Notes
The authors declare no competing financial interests.

■ REFERENCES

(1) Qian, H.; Zhu, M.; Wu, Z.; Jin, R. Quantum Sized Gold Nanoclusters with Atomic Precision. *Acc. Chem. Res.* **2012**, *45*, 1470–1479.

(2) Yang, H.; Wang, Y.; Huang, H.; Gell, L.; Lehtovaara, L.; Malola, S.; Häkkinen, H.; Zheng, N. All-Thiol-Stabilized Ag_{44} and $Au_{12}Ag_{32}$ Nanoparticles with Single-Crystal Structures. *Nat. Commun.* **2013**, *4*, 2422.

(3) Sivaramakrishnan, S.; Chia, P.-J.; Yeo, Y.-C.; Chua, L.-L.; Ho, P. K. H. Controlled Insulator-to-Metal Transformation in Printable Polymer Composites with Nanometal Clusters. *Nat. Mater.* **2007**, *6*, 149–155.

(4) Arenz, M.; Landman, U.; Heiz, U. CO Combustion on Supported Gold Clusters. *Chem. Phys. Chem.* **2006**, *7*, 1871–1879.

(5) Zhu, Y.; Qian, H.; Drake, B. A.; Jin, R. Atomically Precise $Au_{25}(SR)_{18}$ Nanoparticles as Catalysts for the Selective Hydrogenation of α,β-Unsaturated Ketones and Aldehydes. *Angew. Chem., Int. Ed.* **2010**, *49*, 1295–1298.

(6) Häkkinen, H. The Gold-Sulfur Interface at the Nanoscale. *Nat. Chem.* **2012**, *4*, 443–455.

(7) Xavier, P. L.; Chaudhari, K.; Baksi, A.; Pradeep, T. Protein-Protected Luminescent Noble Metal Quantum Clusters: an Emerging Trend in Atomic Cluster Nanoscience. *Nano Rev.* **2012**, *3*, 14767.

(8) Diez, I.; Ras, R. H. A. Fluorescent Silver Nanoclusters. *Nanoscale* **2011**, *3*, 1963–1970.

(9) Geim, A. K. Graphene: Status and Prospects. *Science* **2009**, *324*, 1530–1534.

(10) Castro, N. A. H.; Guinea, F.; Peres, N. M. R.; Novoselov, K. S.; Geim, A. K. The Electronic Properties of Graphene. *Rev. Mod. Phys.* **2009**, *81*, 109–162.

(11) Berger, C.; Song, Z.; Li, T.; Li, X.; Ogbazghi, A. Y.; Feng, R.; Dai, Z.; Marchenkov, A. N.; Conrad, E. H.; First, P. N.; de Heer, W. A. Ultrathin Epitaxial Graphite: Two-Dimensional Electron Gas Properties and a Route Toward Graphene-Based Nanoelectronics. *J. Phys. Chem. B* **2004**, *108*, 19912–19916.

(12) Novoselov, K. S.; Geim, A. K.; Morozov, S. V.; Jiang, D.; Zhang, Y.; Dubonos, S. V.; Grigorieva, I. V.; Firsov, A. A. Electric Field Effect in Atomically Thin Carbon Films. *Science* **2004**, *306*, 666–669.

(13) Miller, D. L.; Kubista, K. D.; Rutter, G. M.; Ruan, M.; de Heer, W. A.; Kindermann, M.; First, P. N.; Stroscio, J. A. Real-Space Mapping of Magnetically Quantized Graphene States. *Nat. Phys.* **2010**, *6*, 811–817.

(14) Yin, P. T.; Kim, T.-H.; Choi, J.-W.; Lee, K.-B. Prospects for Graphene-Nanoparticle-Based Hybrid Sensors. *Phys. Chem. Chem. Phys.* **2013**, *15*, 12785–12799.

(15) Wang, C.; Li, J.; Amatore, C.; Chen, Y.; Jiang, H.; Wang, X.-M. Gold Nanoclusters and Graphene Nanocomposites for Drug Delivery and Imaging of Cancer Cells. *Angew. Chem., Int. Ed.* **2011**, *50*, 11644–11648.

(16) Sreeprasad, T. S.; Maliyekkal, S. M.; Lisha, K. P.; Pradeep, T. Reduced Graphene Oxide-Metal/Metal Oxide Composites: Facile Synthesis and Application in Water Purification. *J. Hazard. Mater.* **2011**, *186*, 921–931.

(17) Luedtke, W. D.; Landman, U. Slip Diffusion and Levy Flights of an Adsorbed Gold Nanocluster. *Phys. Rev. Lett.* **1999**, *82*, 3835–3838.

(18) Yoon, B.; Luedtke, W. D.; Gao, J.; Landman, U. Diffusion of Gold Clusters on Defective Graphite Surfaces. *J. Phys. Chem. B* **2003**, *107*, 5882−5891.

(19) Cretu, O.; Krasheninnikov, A. V.; Rodriguez-Manzo, J. A.; Sun, L.; Nieminen, R. M.; Banhart, F. Migration and Localization of Metal Atoms on Strained Graphene. *Phys. Rev. Lett.* **2010**, *105*, 196101−196104.

(20) Zhou, W.; Kapetanakis, M. D.; Prange, M. P.; Pantelides, S. T.; Pennycook, S. J.; Idrobo, J.-C. Direct Determination of the Chemical Bonding of Individual Impurities in Graphene. *Phys. Rev. Lett.* **2012**, *109*, 206801−206805.

(21) Binz, S. M.; Hupalo, M.; Liu, X.; Wang, C. Z.; Lu, W.-C.; Thiel, P. A.; Ho, K. M.; Conrad, E. H.; Tringides, M. C. High Island Densities and Long Range Repulsive Interactions: Fe on Epitaxial Graphene. *Phys. Rev. Lett.* **2012**, *109*, 26101−26105.

(22) Wang, B.; Yoon, B.; Koenig, M.; Fukamori, Y.; Esch, F.; Heiz, U.; Landman, U. Size-Selected Monodisperse Nanoclusters on Supported Graphene: Bonding, Isomerism, and Mobility. *Nano Lett.* **2012**, *12*, 5907−5912.

(23) Shichibu, Y.; Negishi, Y.; Tsunoyama, H.; Kanehara, M.; Teranishi, T.; Tsukuda, T. Extremely High Stability of Glutathionate-Protected Au_{25} Clusters Against Core Etching. *Small* **2007**, *3*, 835−839.

(24) Ramakrishna, G.; Varnavski, O.; Kim, J.; Lee, D.; Goodson, T. Quantum-Sized Gold Clusters as Efficient Two-Photon Absorbers. *J. Am. Chem. Soc.* **2008**, *130*, 5032−5033.

(25) Zhu, M.; Aikens, C. M.; Hendrich, M. P.; Gupta, R.; Qian, H.; Schatz, G. C.; Jin, R. Reversible Switching of Magnetism in Thiolate-Protected Au_{25} Superatoms. *J. Am. Chem. Soc.* **2009**, *131*, 2490−2492.

(26) Wu, Z.; Jin, R. On the Ligand's Role in the Fluorescence of Gold Nanoclusters. *Nano Lett.* **2010**, *10*, 2568−2573.

(27) Das, A.; Li, T.; Nobusada, K.; Zeng, C.; Rosi, N. L.; Jin, R. Nonsuperatomic $[Au_{23}(SC_6H_{11})_{16}]$- Nanocluster Featuring Bipyramidal Au_{15} Kernel and Trimeric $Au_3(SR)_4$ Motif. *J. Am. Chem. Soc.* **2013**, *135*, 18264−18267.

(28) Heaven, M. W.; Dass, A.; White, P. S.; Holt, K. M.; Murray, R. W. Crystal Structure of the Gold Nanoparticle $[N(C_8H_{17})_4]$-$[Au_{25}(SCH_2CH_2Ph)_{18}]$. *J. Am. Chem. Soc.* **2008**, *130*, 3754−3755.

(29) Zhu, M.; Aikens, C. M.; Hollander, F. J.; Schatz, G. C.; Jin, R. Correlating the Crystal Structure of a Thiol-Protected Au_{25} Cluster and Optical Properties. *J. Am. Chem. Soc.* **2008**, *130*, 5883−5885.

(30) Zeng, C.; Qian, H.; Li, T.; Li, G.; Rosi, N. L.; Yoon, B.; Barnett, R. N.; Whetten, R. L.; Landman, U.; Jin, R. Total Structure and Electronic Properties of the Gold Nanocrystal $Au_{36}(SR)_{24}$. *Angew. Chem., Int. Ed.* **2012**, *51*, 13114−13118.

(31) Qian, H.; Eckenhoff, W. T.; Zhu, Y.; Pintauer, T.; Jin, R. Total Structure Determination of Thiolate-Protected Au_{38} Nanoparticles. *J. Am. Chem. Soc.* **2010**, *132*, 8280−8281.

(32) Jadzinsky, P. D.; Calero, G.; Ackerson, C. J.; Bushnell, D. A.; Kornberg, R. D. Structure of a Thiol Monolayer-Protected Gold Nanoparticle at 1.1 Å Resolution. *Science* **2007**, *318*, 430−433.

(33) Walter, M.; Häkkinen, H. Optical Absorption of Magnesia-Supported Gold Clusters and Nanoscale Catalysts: Effects Due to the Support, Clusters, and Adsorbants. *Phys. Rev. B: Condens. Matter Mater. Phys.* **2005**, *72*, 205440−205445.

(34) Yoon, B.; Haekkinen, H.; Landman, U.; Woerz, A. S.; Antonietti, J.-M.; Abbet, S.; Judai, K.; Heiz, U. Charging Effects on Bonding and Catalyzed Oxidation of CO on Au_8 Clusters on MgO. *Science* **2005**, *307*, 403−407.

(35) Moseler, M.; Häkkinen, H.; Landman, U. Supported Magnetic Nanoclusters: Soft Landing of Pd Clusters on a MgO Surface. *Phys. Rev. Lett.* **2002**, *89*, 176101−176104.

(36) Dreyer, D. R.; Park, S.; Bielawski, C. W.; Ruoff, R. S. The Chemistry of Graphene oxide. *Chem. Soc. Rev.* **2010**, *39*, 228−240.

(37) Dass, A.; Stevenson, A.; Dubay, G. R.; Tracy, J. B.; Murray, R. W. Nanoparticle MALDI-TOF Mass Spectrometry Without Fragmentation: $Au_{25}(SCH_2CH_2Ph)_{18}$ and Mixed Monolayer $Au_{25}(SCH_2CH_2Ph)_{18-x}(L)_x$. *J. Am. Chem. Soc.* **2008**, *130*, 5940−5946.

(38) Shibu, E. S.; Muhammed, M. A. H.; Tsukuda, T.; Pradeep, T. Ligand Exchange of $Au_{25}SG_{18}$ Leading to Functionalized Gold Clusters: Spectroscopy, Kinetics, and Luminescence. *J. Phys. Chem. C* **2008**, *112*, 12168−12176.

(39) Chakraborty, I.; Govindarajan, A.; Erusappan, J.; Ghosh, A.; Pradeep, T.; Yoon, B.; Whetten, R. L.; Landman, U. The Superstable 25 kDa Monolayer Protected Silver Nanoparticle: Measurements and Interpretation as an Icosahedral $Ag_{152}(SCH_2CH_2Ph)_{60}$ Cluster. *Nano Lett.* **2012**, *12*, 5861−5866.

(40) Baksi, A.; Xavier, P. L.; Chaudhari, K.; Goswami, N.; Pal, S. K.; Pradeep, T. Protein-Encapsulated Gold Cluster Aggregates: the Case of Lysozyme. *Nanoscale* **2013**, *5*, 2009−2016.

(41) Qian, H.; Jin, R. Controlling Nanoparticles with Atomic Precision: The Case of $Au_{144}(SCH_2CH_2Ph)_{60}$. *Nano Lett.* **2009**, *9*, 4083−4087.

(42) Ramasamy, P.; Guha, S.; Shibu, E. S.; Sreeprasad, T. S.; Bag, S.; Banerjee, A.; Pradeep, T. Size Tuning of Au Nanoparticles Formed by Electron Beam Irradiation of Au_{25} Quantum Clusters Anchored Within and Outside of Dipeptide Nanotubes. *J. Mater. Chem.* **2009**, *19*, 8456−8462.

(43) Hansen, J.-P.; McDonald, I. R. *Theory of Simple Liquids*; Academic: London, 1986.

F

dx.doi.org/10.1021/jp503001s | *J. Phys. Chem. C* XXXX, XXX, XXX−XXX